

# Improved reconstruction for compressive hyperspectral imaging using spatial-spectral non-local means regularization

Pablo Meza, Department of Electrical Engineering, University of La Frontera, Temuco, Chile

Esteban Vera, Department of Electrical and Computer Engineering, Duke University, Durham, USA

Javier Martinez, Department of Electrical Engineering, University of La Frontera, Temuco, Chile

## Abstract

*Compressive sensing has emerged as a novel sensing theory that can override the Shannon-Nyquist limit, having powerful implications in reducing the dimensionality of hyperspectral imaging acquisition demands. In order to recover the hyperspectral datacube from limited optically compressed measurements, we present a new reconstruction algorithm that exploits the space and spectral correlations through non-local means regularization. Based on a simple compressive sensing hyperspectral architecture that uses a digital micromirror device and a spectrometer, the reconstruction process is solved with the help of split Bregman optimization techniques, including penalty functions defined according to the spatial and spectral properties of the scene and noise sources.*

## Introduction

Most visible (VIS) and near infrared (NIR) spectrometers are based on spectral dispersive elements such as prisms or diffraction gratings, providing the spectral power distribution of the sample [1]. However, spectrometers with different optical systems have been proposed over the years, seeking to improve performance in terms of temporal, spatial and spectral resolution, signal-to-noise ratio (SNR) ratio and portability [2]. Conventional spectrometers are based on a linear detector array, which converts the spectrally decomposed incoming radiation, from a single spatial point, into digital counts. Hyperspectral imaging (HSI) is the extension into the spatial domain of the spectrometer optical properties. The acquired data is a two-dimensional spatial array of vectors that contain the spectral signature for the respective spatial measurements; this three-dimensional data structure is better known as a hypercube [3]. HSI is a powerful tool, but its high dimensionality makes the data acquisition process cumbersome and demanding. In this sense, compressive sensing (CS) has emerged in recent years as a novel sensing theory that goes beyond the Shannon-Nyquist limit, having powerful implications in the design of optical imaging devices [4].

CS states that an  $N$ -pixel image of an object can be reconstructed from a set of  $M < N$  linear measurements (e.g. random projections) by exploiting the sparsity found in signals [5]. Since CS requires fewer measurements, it can be applied to reduce the number of detector elements needed for imaging systems. Imaging via CS was experimentally demonstrated by Takhar et al. using a novel camera architecture that employs a digital micromirror device (DMD) and a single photodiode sensor [6]. Further, Gehm et al. [7] proposed a spectral imager design where the optical scheme used two prisms as spectral dispersive elements, putting a coded aperture between. Later, Wagadarikar et al. [8] presented

a more simple design by omitting one prism. Sun and Kelly follows the scheme proposed by Takhar et al., replacing the photodiode with a spectrometer, converting the original single-pixel camera into a compressive hyperspectral imager [9]. From now on we will focus on the CS imaging scheme proposed by Sun and Kelly due to its simplicity and the potential in the reuse of spectral equipment.

Once the signal is acquired, sparse recovery algorithms are used to estimate the image when the number of unknowns,  $N$ , is much larger than the number of observations,  $M$  [10]. This is an ill-posed problem as there are a possibly infinite number of candidate solutions; nevertheless, CS theory provides a set of conditions that, if satisfied, assure an accurate estimation of the image [5]. Some well known algorithms are basis pursuit with inequality constraints, dantzig selector, and cross validation [11–13]. The experimental results have shown that CS imaging is sensitive not only to the selection of sparsity bases but also to noise sources. As any practical imaging device, CS hyperspectral imagers are affected by blurring due to lens imperfections, inhomogeneous pixel responsivities and limited spectral responsivity on the lower and higher spectral bands [14, 15]. Further, photodetector's dark current introduces a fixed offset noise per pixel and the readout electronics introduces temporal noise [16, 17]. Also, due to the required spectral dispersive elements, the energy level of the incoming radiation is divided by the number of spectral bands acquired, lowering even more the SNR per band and degrading the quality of the rendered spectral images. This is why the use of prior information, beyond pure sparsity, is a mandatory task during the acquisition and recovery process. In this sense, total variation (TV) edge preserving regularization scheme have been successfully coupled to CS recovery by assuming that the gradient of the signal or image is sparse [38]. However, TV minimization has been proven to be difficult to resolve and various approaches have been proposed, to name a few, L1-Magic, TwIST, NESTA, and TVAL3 [18–20]. Other priors, like wavelet-based metrics or non-local means (NLM), are used with the TV approach to compensate for the noise by assuming spatial redundancy in the scene [21]. In particular, Zhang et al. exploited the spatial correlation of the scene by proposing a CS recovery algorithm based on the spatial NLM prior [22].

The fact of hyperspectral images being often highly correlated, not only in the spatial domain but also between spectral bands, should be exploited during the CS recovery [23]. In order to do this, a recovery algorithm is presented as an optimization problem that includes a modified NLM spatial-spectral regularization term, solved using split Bregman techniques, delivering estimated images with higher fidelities from fewer measurements.

We present results using hyperspectral imagery obtained through an experimental setup based on a push-broom hyperspectral camera (PBHC), showing a competitive performance compared with Li's TVAL3 state-of-the-art method [20]. The rest of this article is structured as follows. First, the mathematical derivations for the proposed algorithm are developed. Second, the metrics to evaluate the performance of the algorithms are described. Third, the experimental results using synthetic datasets are introduced. Finally, the conclusions and future trends for this work are presented.

## Proposed Algorithm

In the CS imaging scheme proposed by Sun and Kelly [9], each detector acquires a narrow spectral band of CS spatial measurements. Since each detector has a different response due to the presence of noise variable in time, the acquired detector response is modeled by:

$$f_k = \Phi u_k + \eta_k, \quad (1)$$

where  $\Phi$  represent the random projection matrix and  $u_k$  correspond to a 2D spatial image, reshaped in a vector form, at the  $k$ -th spectral channel. The parameter  $\eta_k$  corresponds to the noise column, usually defined as a random zero-mean Gaussian noise. Finally,  $f_k$  corresponds to the acquired compressive measurements. Due to the ill-posed nature of the problem, the reconstruction of the data is tackled as a  $l_1$ -norm optimization problem, subjected to some restriction, usually reformulated with inequality constrains [24]. Further, when working with piecewise smooth spectral images, the  $l_1$ -norm in Eq. (1) can be replaced by the TV semi-norm of the signal as follows:

$$\min_{u_k \in \mathbb{R}^{N \times 1}} \|u_k\|_{TV} \quad \text{s.t.} \quad f_k = \Phi u_k \quad (2)$$

The TV semi-norm enforces sparsity for the image gradient and can be calculated using the following anisotropic model:

$$\|u_k\|_{TV} = |\nabla_x u_k| + |\nabla_y u_k|. \quad (3)$$

However, this traditional approach only exploit the information acquired at the  $k$ -th spectral band, without considering the information available on the other spectral bands.

To exploit the spatial-spectral redundancy observed in single-DMD CS schemes, Eq.(2) is coupled with a spatial-spectral NLM regularization as follows:

$$\min_{u_k \in \mathbb{R}^{N \times 1}} \|u_k\|_{TV} + \frac{\alpha}{2} \|u_k - \sum_{l=1}^L W_{kl} u_l\|_2^2 \quad \text{s.t.} \quad f_k = \Phi u_k, \quad (4)$$

where  $l = 1, \dots, k, \dots, L$ . The NLM regularization compensates the presence of noise while maintaining the edges and the fine texture image details. It is based on the assumption that is likely to have redundant spatial information in the scene. However, the expression has been modified to take into account any spectral redundancy by comparing and averaging spatial-spectral neighborhood patches. Each element of the data matrix  $W_{kl}$  is obtained as follows:

$$W_{kl} = \begin{cases} w_{kl}(i, j) & : j \in O_i \\ 0 & : \text{otherwise,} \end{cases} \quad (5)$$

where  $w_{kl}(i, j)$  is the weight component calculated as:

$$w_{kl}(i, j) = \frac{1}{Z_k(i)} \exp\left(\frac{\|u_k(O_i) - u_l(O_j)\|_{2,g}^2}{h^2}\right), \quad (6)$$

$$Z_k(i, j) = \sum_l \sum_j \exp\left(\frac{\|u_k(O_i) - u_l(O_j)\|_{2,g}^2}{h^2}\right). \quad (7)$$

The suffixes  $i$  and  $j$  denote the center pixel of the reference patch and the center pixel of the patches to be compared, respectively. Therefore,  $u_l(O_i)$  defines the column vector that contains the pixels of the image patch, at the  $l$ -th spectral channel, in a square neighborhood of fixed size  $O_i$  centered at the  $i$ -th position. The term  $h^2$  is known as the NLM filtering parameter, usually set equal to the standard deviation of the noise. Also,  $\|\cdot\|_{2,g}^2$  stands for the Euclidean distance and  $g$  for the standard deviation of the Gaussian kernel that imposes a decaying weight to pixels away from the patch center. In order to minimize Eq. (4), a split Bregman approach have been used, redefining the expression without constraints and replacing the TV with auxiliary variables ( $d_{x,k} = \nabla_x u_k$  and  $d_{y,k} = \nabla_y u_k$ ). This is done by iteratively solving the unconstrained problem, and then modifying the value of  $u_k, d_{x,k}, d_{y,k}$  used in the next iteration.

$$\begin{aligned} (u_k^{p+1}, d_{x,k}^{p+1}, d_{y,k}^{p+1}) &= \min_{u_k, d_{x,k}, d_{y,k}} |d_{x,k}| + |d_{y,k}| + \\ &\frac{\alpha}{2} \|u_k - \sum_{l=1}^L W_{kl} u_l\|_2^2 + \frac{\beta}{2} \|\Phi u_k - f_k + c_k^p\|_2^2 + \\ &\frac{\gamma}{2} \|\nabla_x u_k - d_{x,k}^p + e_{x,k}^p\|_2^2 + \frac{\gamma}{2} \|\nabla_y u_k - d_{y,k}^p + e_{y,k}^p\|_2^2 \end{aligned} \quad (8)$$

$$c_k^{p+1} = c_k^p + (\Phi u_k^{p+1} - f_k^{p+1}) \quad (9)$$

$$e_{x,k}^{p+1} = e_{x,k}^p + (\nabla_x u_k^{p+1} - d_{x,k}^{p+1}) \quad (10)$$

$$e_{y,k}^{p+1} = e_{y,k}^p + (\nabla_y u_k^{p+1} - d_{y,k}^{p+1}) \quad (11)$$

## Image Quality Metrics

Two metrics were selected to evaluate the performance of the CS reconstruction algorithms: i) the root mean-squared error (RMSE) and ii) the roughness ( $\rho$ ) metric. The first metric, RMSE, is used to quantify the distortions between the corresponding ground-truth reference and the estimated image. The mathematical representation of the metric is:

$$RMSE(\hat{u}, u) = \left[ \frac{1}{N} \sum_{n=1}^N (\hat{u}(n) - u(n))^2 \right]^{\frac{1}{2}}. \quad (12)$$

a low RMSE value indicate that the estimated image is closer to the reference. The second metric is the roughness ( $\rho$ ) and measures the amount of image details in the spatial domain. The  $\rho$  metric does not used a reference image, unlike the RMSE, and is calculated as follows:

$$\rho(\hat{u}) = \frac{\|h * \hat{u}\| + \|h^T * \hat{u}\|}{\|\hat{u}\|}, \quad (13)$$

where  $h$  is defined as  $[1 \ -1]$ , the symbol  $*$  correspond to the convolution and  $\|\cdot\|$  to the  $l_1$ -norm. For the  $\rho$  metric, a value close to zero indicates that the image is smooth, with lower presence of noise and artefacts, since both effects increases the high frequency content of the scene.

## Experimental Results

The hyperspectral images used to test the performance of the proposed CS algorithm were obtained through an experimental setup based on a Photonfocus Hurricane 40 V10E PBHC. The camera has a CMOS array composed of  $1024 \times 1024$  pixels, coupled with a spectrograph that record 574 spectral bands at a resolution of 1.04 [nm], between 400 to 1000 [nm]. The experimental setup includes also a mobile platform to emulates the along-track scanning procedure. The platform was configured in order to take 800 time samples, along a spatial trajectory that happens to be orthogonal to the dimension used to encode the spectral information. The scene is illuminated with a calibrated quartz tungsten halogen (QTH) lamp that guarantees an uniform and continuous spectral illumination between 200-2500 [nm]. Also, a two-point calibration procedure was conducted in order to add a specific amount of synthetic noise during the simulations. The calibration device employed here was a Spectralon SRT-99-120, which ensures a diffuse reflectance of 99% in the range of 250 to 2000 [nm]. The experimental setup is presented in Fig. 1.

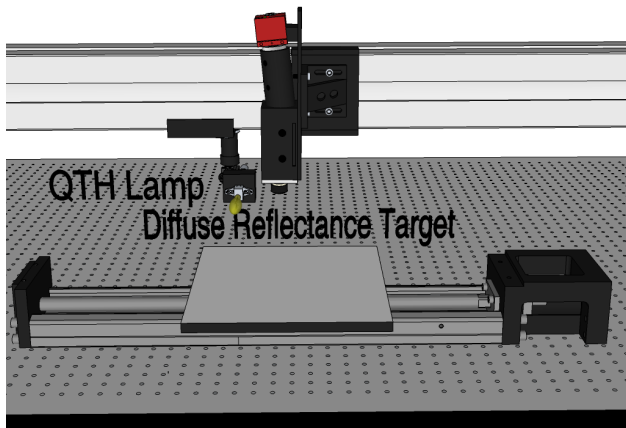


Figure 1: Experimental setup based on a Photonfocus Hurricane 40 V10E PBHC.

Two cropped hypercubes, I and II, were acquired as shown in Fig. 1(b). Both image segments have a size of  $128 \times 128$  pixels in order to reduce simulation time. Consequently, the acquired hypercubes have a dimension of  $128 \times 574 \times 128$  in the spatial, spectral, and temporal domain, respectively. The acquired scenes are presented in Fig. 2.

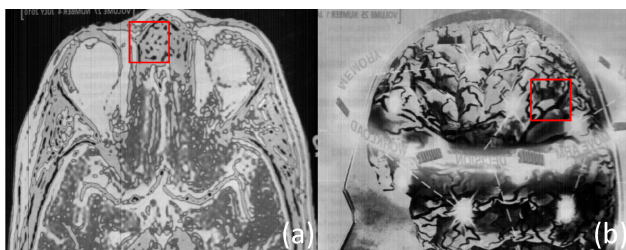


Figure 2: Sample images at 790 [nm] from the acquired hypercubes. The two red squares depicted the cropped hypercube a)I and b)II.

Synthetic random Gaussian noise, defined as 30% of the dynamic range, was added to each spectral image to simulate the acquisition performed by the CS imaging scheme proposed by Sun

and Kelly [9]. For the simulations, the matrix  $\Phi$  was constructed as a Gaussian random projection matrix, considering a 40% of compression ratio.

As aforementioned, the proposed algorithm is compared with the well known TVAL3 method [20], which uses only the information recorded in a single spectral band. Since the proposed algorithm is based on exploiting the redundant information recorded in neighboring bands, comparisons using 9 adjacent spectral bands during the recovery are considered as well. Figures 2(a) and (b) corresponds to the  $128 \times 128$  original spectral image at 790 [nm] from the cropped hypercube I and its recovered version using the TVAL3 algorithm, respectively. Figures 2(c) and (d) are the recovered images using the proposed algorithm exploiting the information in 1 and 9 spectral bands, respectively. It can be observed that both algorithms successfully recover the spatial structure of the scene, however, the proposed algorithm using 9 spectral bands produces less artifacts.

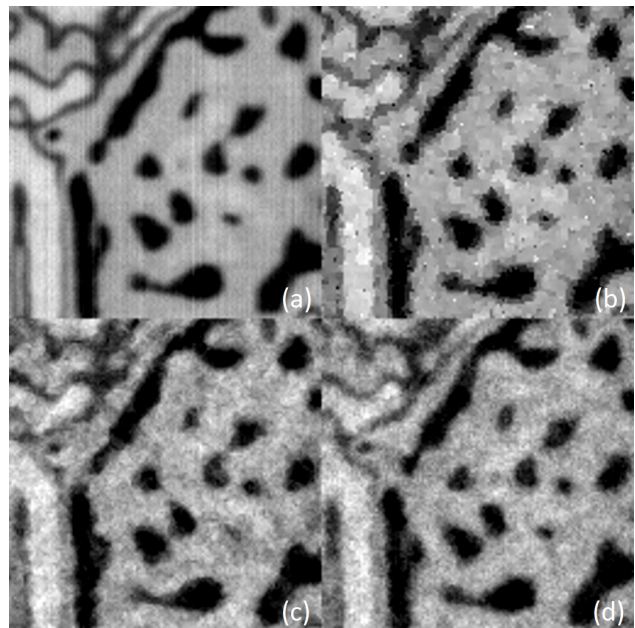


Figure 3: Sample images at 790 [nm] from cropped hypercube I. (a) Original image. Reconstructed images using: (b) TVAL3 algorithm and the proposed algorithm exploiting (c) 1 spectral band and (d) 9 spectral bands.

Table 1 shows comparative results for the recovery algorithms over the cropped hypercube I, affected by synthetic random Gaussian noise. Note that all the metrics values were calculated over the selected region of interest (ROI). Overall, the proposed algorithm provides smaller RMSE values than the TVAL3 algorithm, with the lowest RMSE of 25.77 when using 9 spectral bands. Further, the  $\rho$  metric exhibits that the TVAL3 algorithm and the proposed algorithm produces a general reduction in high-frequency, reaching  $\rho$  values near to the reference image (0.05).

In Fig. 3, the estimated images using the spatial-spectral information from the cropped hypercube II are presented. The image recovered by the TVAL3 algorithm, Fig. 3(b), shows some staircase effect and loss of details. Further, comparing Figs. 3(c) and 3(d), one can assess that both algorithms successfully rendered the spectral images with more defined shapes and fewer

Table 1: Performance metrics for the estimated cropped images I at 790 [nm] using the TVAL3 and the proposed algorithm.

Method	N <sup>o</sup> Bands	RMSE	$\rho$
Reference	1	-	0.05
TVAL3	1	29.69	0.05
Proposed	1	28.08	0.06
Proposed	9	25.77	0.06

artifacts.

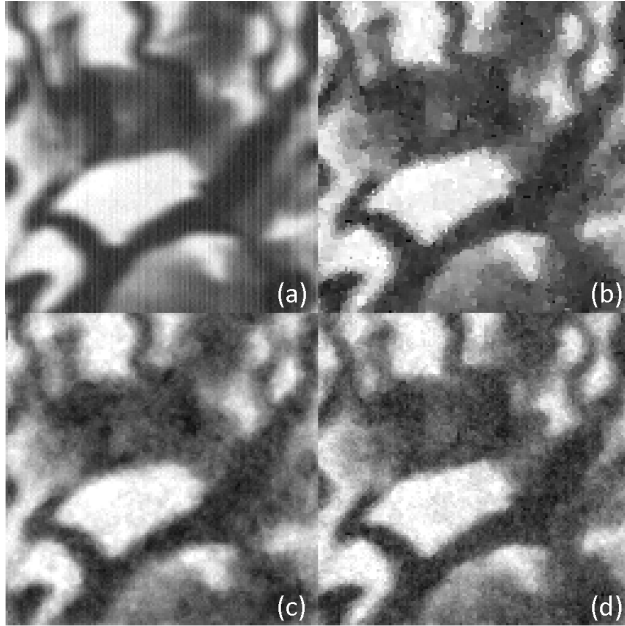


Figure 4: Sample images at 790 [nm] from cropped hypercube II. (a) Original image. Reconstructed images using: (b) TVAL3 algorithm and the proposed algorithm exploiting (c) 1 spectral band and (d) 9 spectral bands.

Table 2 list the performance results of the reconstruction algorithms using single and multiples spectral bands. These results represent an effective reconstruction for the cropped hypercube II. In terms of the RMSE, results show that the proposed method outperforms the TVAL3, achieving a RMSE of 20.76 when 9 adjacent spectral bands are used. Similar results for the algorithms were observed in terms of the  $\rho$ . More precisely, the  $\rho$  value was equal to 0.04 and 0.05 when using the TVAL3 and the proposed algorithm exploiting 9 adjacent spectral bands. Such behavior is due that both algorithms successfully compensate for the random noise, however, the proposed algorithm produces less artifacts.

Table 2: Performance metrics for the estimated cropped images II at 790 [nm] using the TVAL3 and the proposed algorithm.

Method	N <sup>o</sup> Bands	RMSE	$\rho$
Reference	1	-	0.05
TVAL3	1	24.46	0.04
Proposed	1	25.11	0.04
Proposed	9	20.76	0.05

## Conclusions

In this article, we presented a CS reconstruction algorithm following the assumption of spatial-spectral redundancy in CS imaging systems based on Sun and Kelly design [9]. The algorithm incorporates regularization terms based on the assumption that it is likely to observe redundant patches of spatial and spectral information contained in neighboring bands. Here, we have found that the spatial-spectral NLM regularization can fulfill this task, maintaining the spatial-spectral structure of the scene during the reconstruction process, and thus providing better fidelity from fewer measurements.

As a future work, deeper analysis over a greater range of spectral bands will be performed and the adaptability of the proposed algorithm will be verified using the hole spatial information. Also, the reconstruction performed by the proposed algorithm could be improved by selecting a different learning rate for each spectral image according to the acquired spatio-spectral information.

## Acknowledgments

Pablo Meza acknowledges the support of CONICYT, FONDECYT Iniciación Folio 11140605.

## References

- [1] Saleh, B. E. A. and Teich, M. C., [Fundamentals of photonics], vol. 22, Wiley New York (1991).
- [2] Prevatt, J., "Modern uv-vis spectroscopy: A decade of fiber-optic ccd array spectrophotometers," *American laboratory* **36**(15), 28–30 (2004).
- [3] Borengasser, M., Hungate, W. S., and Watkins, R. L., [Hyperspectral Remote Sensing: Principles and Applications], CRC Press (2008).
- [4] Wakin, M., Laska, J., Duarte, M., Baron, D., Sarvotham, S., Takhar, D., Kelly, K., and Baraniuk, R., "An architecture for compressive imaging," in [Image Processing, 2006 IEEE International Conference on], 1273–1276 (Oct 2006).
- [5] Donoho, D., "Compressed sensing," *Information Theory, IEEE Transactions on* **52**, 1289–1306 (April 2006).
- [6] Takhar, D., Laska, J. N., Wakin, M. B., Duarte, M. F., Baron, D., Sarvotham, S., Kelly, K. F., and Baraniuk, R. G., "A new compressive imaging camera architecture using optical-domain compression," in [Proceedings of Computational Imaging IV at SPIE Electronic Imaging], 43–52 (Jan. 2006).
- [7] Gehm, M. E., John, R., Brady, D. J., Willett, R. M., and Schulz, T. J., "Single-shot compressive spectral imaging with a dual-disperser architecture," *Opt. Express* **15**, 14013–14027 (Oct 2007).
- [8] Wagadarikar, A., John, R., Willett, R., and Brady, D., "Single disperser design for coded aperture snapshot spectral imaging," *Appl. Opt.* **47**, B44–B51 (Apr 2008).
- [9] Sun, T. and Kelly, K., "Compressive sensing hyperspectral imager," in [Frontiers in Optics 2009/Laser Science XXV/Fall 2009 OSA Optics & Photonics Technical Digest], CTuA5, Optical Society of America (2009).
- [10] Needell, D. and Tropp, J., "Cosamp: Iterative signal recovery from incomplete and inaccurate samples," *Applied and Computational Harmonic Analysis* **26**(3), 301–321 (2009).
- [11] Chen, S. S., Donoho, D. L., and Saunders, M. A., "Atomic decomposition by basis pursuit," *SIAM Journal on Scientific Computing* **20**(1), 33–61 (1998).

- [12] Candes, E. and Tao, T., "The dantzig selector: Statistical estimation when  $p$  is much larger than  $n$ ," *The Annals of Statistics* **35**(6), 2313–2351 (2007).
- [13] Ward, R., "Compressed sensing with cross validation," *Information Theory, IEEE Transactions on* **55**, 5773–5782 (Dec 2009).
- [14] Gómez-Chova, L., Alonso, L., Guanter, L., Camps-Valls, G., Calpe, J., and Moreno, J., "Correction of systematic spatial noise in push-broom hyperspectral sensors: application to CHRIS/PROBA images," *Appl. Opt.* **47**(28), F46–F60 (2008).
- [15] Acito, N., Diani, M., and Corsini, G., "Signal-dependent noise modeling and model parameter estimation in hyperspectral images," *Geoscience and Remote Sensing, IEEE Transactions on* **49**, 2957–2971 (Aug 2011).
- [16] Gamal, A. E., Fowler, B. A., Min, H., and Liu, X., "Modeling and estimation of fpn components in cmos image sensors," *Proc. SPIE* **3301**, 168–177 (1998).
- [17] Tian, H., Fowler, B., and Gamal, A., "Analysis of temporal noise in cmos photodiode active pixel sensor," *Solid-State Circuits, IEEE Journal of* **36**, 92–101 (Jan 2001).
- [18] Bioucas-Dias, J. and Figueiredo, M., "A new twist: Two-step iterative shrinkage/thresholding algorithms for image restoration," *Image Processing, IEEE Transactions on* **16**, 2992–3004 (Dec 2007).
- [19] Becker, S., Bobin, J., and Candès, E. J., "Nesta: A fast and accurate first-order method for sparse recovery," *SIAM Journal on Imaging Sciences* **4**(1), 1–39 (2011).
- [20] Li, C., Yin, W., Jiang, H., and Zhang, Y., "An efficient augmented lagrangian method with applications to total variation minimization," *Computational Optimization and Applications* **56**(3), 507–530 (2013).
- [21] Buades, A., Coll, B., and Morel, J.-M., "A non-local algorithm for image denoising," in [*Computer Vision and Pattern Recognition, 2005. CVPR 2005. IEEE Computer Society Conference on*], **2**, 60–65 (June 2005).
- [22] Zhang, J., Liu, S., Xiong, R., Ma, S., and Zhao, D., "Improved total variation based image compressive sensing recovery by nonlocal regularization," in [*Circuits and Systems (ISCAS), 2013 IEEE International Symposium on*], 2836–2839 (May 2013).
- [23] Tropp, J. and Gilbert, A., "Signal recovery from random measurements via orthogonal matching pursuit," *Information Theory, IEEE Transactions on* **53**, 4655–4666 (Dec 2007).
- [24] Goldstein, T. and Osher, S., "The split bregman method for 11-regularized problems," *SIAM Journal on Imaging Sciences* **2**(2), 323–343 (2009).

## Author Biography

*Pablo Meza was born on October 6, 1983. He received his B.Sc. in Electronic Engineering and M.S. in Electrical Engineering in 2008, from the University of La Frontera, Chile and his Ph.D. degree in Electrical Engineering in 2014, from the University of Concepcion, Chile. He is currently a full-time Professor of the Electrical Engineering Department at the University of La Frontera. His research activities are focused on signal processing applied to multi- and hyper-spectral imaging systems.*

*Esteban Vera obtained his Bsc, Msc and Phd degrees in Electrical Engineering from the University of Concepcion, Chile, in 1999, 2003 and 2010, respectively. He has worked for the Gemini Observatory and the Very Large Telescope projects. He was a Postdoctoral Research Associate at the University of Arizona. He is currently a Research Scientist at Duke University. His research interests span over computational imaging,*

*signal processing, inverse problems, machine learning, information theory, and astronomical instrumentation.*

*Javier Martnez was born in Chile in 1993. He is currently coursing his B.Sc. degree in Telecommunication Engineering in the University of la Frontera, Chile. He has been working as assistant in the Information Processing Lab since 2015. His main areas of research interest are structured illumination, hyperspectral imaging and compressive sensing.*